NDT&E International 146 (2024) 103156

Contents lists available at ScienceDirect

NDT and E International

journal homepage: www.elsevier.com/locate/ndteint

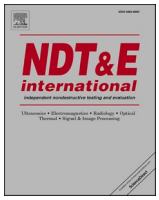

Resolution of multiple semi-infinite delaminations using lock-in infrared thermography

A. Salazar [a,*], D. Sagarduy-Marcos [a], J. Rodríguez-Aseguinolaza [a], A. Mendioroz [a], J.C. Ciria [b], R. Celorrio [c]

[a] Departamento de Física Aplicada, Escuela de Ingeniería de Bilbao, Universidad del País Vasco UPV/EHU, Plaza Ingeniero Torres Quevedo 1, 48013, Bilbao, Spain
[b] Departamento de Informática e Ingeniería de Sistemas, Universidad de Zaragoza, Facultad de Ciencias, c/Pedro Cerbuna 12, 50009, Zaragoza, Spain
[c] Departamento de Matemática Aplicada, EINA/IUMA, Universidad de Zaragoza, Campus Río Ebro, Edificio Torres Quevedo, 50018, Zaragoza, Spain

ARTICLE INFO

Keywords:
Lock-in thermography
Delaminations
Thermal resistance
Nondestructive testing

ABSTRACT

Delaminations are flat subsurface defects parallel to the sample surface. Recently we have demonstrated that lock-in infrared thermography, with optical excitation, allows sizing the geometrical parameters (length, depth and thickness) of a semi-infinite delamination. Here, we analyse the ability of this technique to resolve several parallel and semi-infinite delaminations. First, we develop an analytical method (based on the thermal quadrupoles) together with a numerical formulation to calculate the surface temperature of a sample containing several semi-infinite parallel delaminations. We verify that both methods provide the same temperature values, indicating their consistency. Then, we study the ability of lock-in infrared thermography to resolve two close delaminations. In particular we focus on two main configurations: two non-overshadowed delaminations and two superimposed delaminations. Next, after analysing the inverse problem in terms of residual function minimization, we develop a dedicated parametric estimation procedure able to retrieve the geometry of the studied defects. Finally, we test this procedure with synthetic temperature amplitude and phase data to retrieve the geometrical parameters of both delaminations.

1. Introduction

Active infrared thermography (IRT) with optical excitation is based on stimulating the sample under study by means of a light source and recording the temperature evolution of the sample surface using an infrared video camera [1]. It has been widely applied as a noncontact and nondestructive testing (NDT) tool: anomalies in the surface temperature betray the existence of hidden defects. A very widespread type of defect are delaminations: flat internal defects parallel to the sample surface that appear in layered metals and composites. There is a great interest in detecting them since they reduce the material stiffness and the structure reliability [2].

When looking for flat parallel subsurface defects, a uniform light source is used. Regarding the time profile, one option is using flash lamps or pulsed lasers. The experiment is performed in a few seconds and from the analysis of the time evolution of the surface temperature, the presence of the delamination is revealed. Moreover, the signal processing allows measuring the depth of the delamination [3–8]. In lock-in IRT, instead, continuous lamps or CW lasers are modulated at a given frequency. The lock-in processing of the image sequence for many periods (up to several minutes) provides clean amplitude and phase thermograms from which the delamination depth is estimated [9–11].

As said in the previous paragraph, most published works focused on the delamination detection and depth sizing. Only a few recent works dealt with the measurement of the delamination thickness, i.e. the width of the air layer, or what is equivalent, the thermal resistance of the delamination [12–15]. These papers studied ideal delaminations i.e. of infinite area. Using a 1D model, an analytical solution for the surface temperature of the sample as a function of the depth and thickness of the delamination was obtained. By fitting the experimental data to the 1D

* Corresponding author.
E-mail address: agustin.salazar@ehu.es (A. Salazar).

https://doi.org/10.1016/j.ndteint.2024.103156
Received 18 December 2023; Received in revised form 2 May 2024; Accepted 30 May 2024
Available online 3 June 2024

model, the depth and thickness of real delaminations in composites were measured [13,14].

Recently, with the aim of approaching more realistic cases, we studied semi-infinite delaminations, e.g. with the shape of a rectangle of finite length an infinite width. We solved the heat diffusion equation in 2D for a bulk sample containing a semi-infinite delamination, both analytically (using the thermal quadrupoles method [16]) and numerically (using Finite Element Methods (FEM)). In this way, we obtained the surface temperature as a function of the length, depth and thickness of the delamination [17]. Then, a specifically developed inversion procedure for the delamination geometry minimization problem was designed and accurately deployed in order to retrieve the length, depth and width of the delamination. This inversion procedure was verified by taking lock-in thermography data on metallic samples containing calibrated semi-infinite delaminations [18].

In this work, we have gone a step further and we have analysed the ability of lock-in IRT to resolve several parallel and semi-infinite delaminations. Resolution means whether we can distinguish two close delaminations. For this purpose we have proceeded as follows. First, we found an analytical solution of the heat diffusion equation (based on the thermal quadrupoles) to calculate the surface temperature of a bulk sample containing several semi-infinite parallel delaminations. We have also solved the heat diffusion equation numerically (using FEM) and we verify that both methods give the same temperature values. Then, we have calculated the surface temperature on samples containing two delaminations. For the sake of simplicity we dealt with two interesting configurations: (a) two close non-overshadowed delaminations and (b) two superimposed delaminations. We focus on the capability of the surface temperature to resolve (distinguish) two very close delaminations. Next, we have developed a dedicated inverse parametric estimation strategy to retrieve the geometrical parameters of the delaminations. Due to the small sensitivity of the surface temperature to some of those parameters (mainly length and thickness), and the potential coupling between them, a double step residual minimization procedure is proposed in order to avoid local minima far away from the true solution. Finally, we have applied this procedure to synthetic temperature amplitude and phase data, with added Gaussian noise, to retrieve the geometrical parameters characterizing both delaminations: lengths, depths, thicknesses and the distance between them.

2. Theory

In this section we calculate the surface temperature oscillation of a sample illuminated by a modulated light beam. The sample contains several delaminations buried at different depths. The problem is solved analytically and numerically in order to check the validity of the results.

2.1. Analytical method

Let us consider a parallelepiped and opaque sample with several semi-infinite parallel delaminations. Each of them is buried at a given depth and is infinitely long in the y-direction. Fig. 1 shows the cross-section of the sample. The thickness of the sample is the sum of the thicknesses of each layer $e = e_1 + e_2 + \ldots + e_{n+1}$ and L is the length of the sample along the x-direction. Each delamination is characterized by three parameters: the length $\ell_i = x_i' - x_i$, the depth $d_i = e_1 + e_2 + \ldots + e_i$ and the thermal resistance R_i, which is assumed to be homogeneous. This last quantity, whose meaning is difficult to grasp, is related to the delamination thickness w_i through: $R_i = w_i/K_{air}$, where $K_{air} = 0.025$ $\mathrm{Wm^{-1}K^{-1}}$ is the thermal conductivity of air [19].

The front surface is uniformly illuminated by a continuous light source of intensity I_o modulated at a frequency f ($\omega = 2\pi f$). We assume

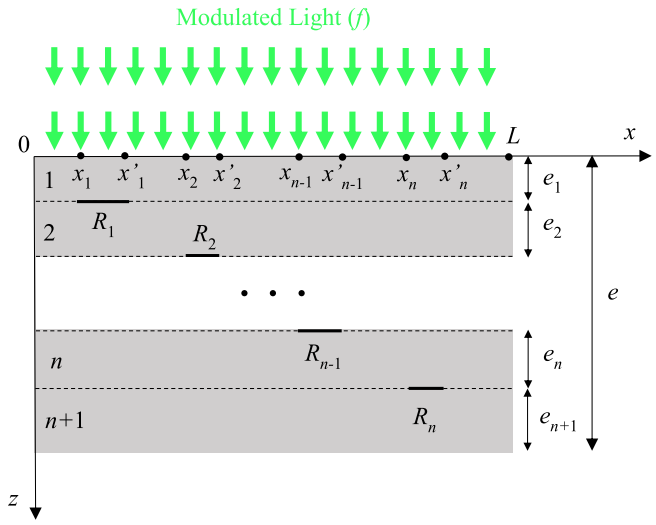

Fig. 1. Cross-section of the opaque sample containing n horizontal delaminations, showing the depth, lateral extent and thermal resistance of each delamination. The dashed lines divide the sample in n+1 layers with the same thermal properties.

adiabatic boundary conditions at the sample surfaces since we demonstrated in a previous work that the influence of heat losses by convection and radiation is negligible at frequencies higher than 0.2 Hz [15].

To simplify the solution of the heat diffusion equation we divide the sample in n+1 layers made of the same material, as shown by dashed lines in Fig. 1. According to the 2D symmetry of the problem, the heat diffusion equation in each layer writes

$$\frac{\partial^2 T_i}{\partial x^2} + \frac{\partial^2 T_i}{\partial z^2} - \frac{1}{D}\frac{\partial T_i}{\partial t} = 0, i = 1, 2, \ldots, n+1 \tag{1}$$

where D is the thermal diffusivity of the sample. Due to the modulated illumination, the temperature of the sample oscillates at the same frequency as the excitation:

$$T_i(x, z, t) = \tau_i(x, z)e^{j\omega t}, \tag{2}$$

where τ is the temperature oscillation when the steady state is reached. By substituting Eq. (2) into Eq. (1) we obtain the following partial differential equation

$$\frac{\partial^2 \tau_i}{\partial x^2} + \frac{\partial^2 \tau_i}{\partial z^2} - \frac{j\omega}{D}\tau = 0. \tag{3}$$

Finding the surface temperature oscillation for the geometry shown in Fig. 1 requires solving Eq. (3) with the following boundary conditions: adiabatic boundary conditions at all free surfaces, modulated illumination at the sample surface, together with heat flux continuity and temperature jump at the interfaces.

The constitutive Eq. (3) along with the set of boundary conditions can be solved by using the cosine Fourier transform of the x-coordinate of τ (x, z)

$$\theta_i(\alpha_p, z) = \int_0^L \tau_i(x, z)\cos(\alpha_p x)dx, \text{ with } \alpha_p = \frac{p\pi}{L} \text{ and } p \in N, \tag{4}$$

where $\theta_i(\alpha_p, z)$ is the cosine Fourier transform of $\tau_i(x,z)$. In this way, and using the thermal quadrupoles formalism (see p. 246 in Ref. [16]), we obtain a matrix expression for the surface temperature and heat flux in the cosine Fourier space

$$\begin{pmatrix}\theta_1(0)\\ \Phi_1(0)\end{pmatrix}=\begin{pmatrix}A_1 & B_1\\ C_1 & A_1\end{pmatrix}\begin{pmatrix}I & N_\rho^1\\ 0 & I\end{pmatrix}\begin{pmatrix}A_2 & B_2\\ C_2 & A_2\end{pmatrix}\begin{pmatrix}I & N_\rho^2\\ 0 & I\end{pmatrix}\begin{pmatrix}A_3 & B_3\\ C_3 & A_3\end{pmatrix}\cdots\begin{pmatrix}I & N_\rho^m\\ 0 & I\end{pmatrix}\begin{pmatrix}A_{n+1} & B_{n+1}\\ C_{n+1} & A_{n+1}\end{pmatrix}\begin{pmatrix}\theta_{n+1}(e)\\ \Phi_{n+1}(e)\end{pmatrix}, \tag{5}$$

where Φ_i is the cosine Fourier transform of the heat flux. $\theta_1(0), \theta_{n+1}(e)$, $\Phi_1(0)$ and $\Phi_{n+1}(e)$ are column vectors of length N+1, where N is high enough to guarantee convergence. Note that in $\Phi_1(0)$ only the first term is no null and equal to $I_oL/2$, whereas $\Phi_{n+1}(e)$ is the null vector. I is the unit square matrix of size N+1. A_i, B_i and C_i are diagonal square matrices of size N+1 whose coefficients are $\cosh(\gamma_p e_i)$, $\sinh(\gamma_p e_i)/(K\gamma_p)$ and $K\gamma_p\sinh(\gamma_p e_i)$, respectively. Here, K is the sample thermal conductivity and $\gamma_p^2 = \alpha_p^2 + j\omega/D$. Finally, the coefficients of the square matrix N_ρ^i contain the information on the thermal resistance of the delaminations

$$N_\rho^i=\frac{1}{L}\begin{pmatrix}\rho_o^i & 2\rho_1^i & 2\rho_2^i & \cdots & 2\rho_N^i\\ \rho_1^i & \rho_o^i+\rho_2^i & \rho_1^i+\rho_3^i & \cdots & \rho_{N-1}^i+\rho_{N+1}^i\\ \rho_2^i & \rho_1^i+\rho_3^i & \rho_0^i+\rho_4^i & \cdots & \rho_{N-2}^i+\rho_{N+2}^i\\ \cdots & \cdots & \cdots & \cdots & \cdots\\ \rho_N^i & \rho_{N-1}^i+\rho_{N+1}^i & \rho_{N-2}^i+\rho_{N+2}^i & \cdots & \rho_o^i+\rho_{2N}^i\end{pmatrix} \tag{6}$$

where each coefficient, in the case of uniform thermal resistances is given by

$$\rho_o^i=R_i\left(x_i^{'}-x_i\right), \tag{7a}$$

$$\rho_p^i=\frac{R_i}{\alpha_p}\left[\sin\left(\alpha_p x_i^{'}\right)-\sin\left(\alpha_p x_i\right)\right]\quad \text{for } p\neq 0 \tag{7b}$$

The real surface temperature oscillation, $\tau_1(x, 0)$, is obtained by performing an inverse cosine Fourier transform of $\theta_1(0)$, which is given by (see p. 159 in Ref. [16])

$$\tau_1(x,0)=\frac{1}{L}\theta_1(\alpha_o,0)+\frac{2}{L}\sum_{p=1}^{\infty}\theta_1\left(\alpha_p,0\right)\cos\left(\alpha_p\right). \tag{8}$$

For the sake of simplicity, in the remaining of the paper we will name τ just as temperature.

In this manuscript we will deal with a sample containing two delaminations with null heat flux at the rear surface ($z = e$), so Eq. (5) reduces to

$$\begin{pmatrix}\theta_1(0)\\ \Phi_1(0)\end{pmatrix}=\begin{pmatrix}A_1 & B_1\\ C_1 & A_1\end{pmatrix}\begin{pmatrix}I & N_\rho^1\\ 0 & I\end{pmatrix}\begin{pmatrix}A_2 & B_2\\ C_2 & A_2\end{pmatrix}\begin{pmatrix}I & N_\rho^2\\ 0 & I\end{pmatrix}\begin{pmatrix}A_3 & B_3\\ C_3 & A_3\end{pmatrix}\begin{pmatrix}\theta_3(e)\\ 0\end{pmatrix}=\begin{pmatrix}A & B\\ C & D\end{pmatrix}\begin{pmatrix}A_3\theta_3(e)\\ C_3\theta_3(e)\end{pmatrix}, \tag{9}$$

where

$$\begin{pmatrix}A & B\\ C & D\end{pmatrix}=\prod_{i=1}^{2}\begin{pmatrix}A_i & B_i\\ C_i & A_i\end{pmatrix}\begin{pmatrix}I & N_\rho^i\\ 0 & I\end{pmatrix}. \tag{10}$$

Moreover, if the sample is very thick, $e_3 \to \infty$, both $\cosh(\gamma_p e_3)$ and $\sinh(\gamma_p e_3)$ tend to $\exp(\gamma_p e_3)/2$, and $C_3 \to KGA_3$. Accordingly, Eq. (9) can be written as

$$\begin{pmatrix}\theta_1(0)\\ \Phi_1(0)\end{pmatrix}=\begin{pmatrix}A & B\\ C & D\end{pmatrix}\begin{pmatrix}A_3\theta_3(e)\\ KGA_3\theta_3(e)\end{pmatrix}, \tag{11}$$

where G is a diagonal square matrix of size N+1 whose coefficients are γ_p. Finally, the cosine Fourier transform of the surface temperature is given by

$$\begin{aligned}\theta_1(0)&=[A+KBG]A_3A_3^{-1}[C+KDG]^{-1}\Phi_1(0)\\ &=[A+KBG][C+KDG]^{-1}\Phi_1(0).\end{aligned} \tag{12}$$

Note that the term A_3 and consequently any dependence on e_3 disappears. In Ref. [16] we already discussed the instability problems associated to the quadrupoles method and the way to overcome them. Here, the size N+1 of the matrices in Eq. (12) is taken as high as 1000 to guarantee precision in the calculation of the temperature oscillation. In this way, a temperature profile along the x-axis takes 5 min using a desktop PC (3.6 GHz, 16 GB of RAM).

2.2. Numerical method

Conventional heat diffusion equation ($D\nabla^2 T = \partial T/\partial t$) has been numerically solved by using the Finite Element Method (FEM) together with adiabatic boundaries for the non-illuminated surfaces and harmonically modulated illumination ($\frac{I_o}{2}\cos(\omega t)$) at $z = 0$. The defect has been introduced as a 2-D thermal contact resistance characterized by the heat flux continuity and a temperature jump ($\Delta T|_{z=di} = KR_i\nabla T$). In order to avoid very fine meshes, the delaminations are introduced in the domain as 2-D planar contact interfaces with thermal resistances R_i. Considering the nature of the applied boundary conditions over the defect, the mesh nodes corresponding to the delamination are duplicated maintaining spatially coincident coordinates ensuring the continuity of the spatial discretization.

Although this FEM modelling strategy is general and would allow the computation over any 3-D domain, in this work, taking advantage of the considered problem symmetry, the delaminations are introduced over the cross sectional domain shown in Fig. 1 as 1-D geometries. The numerical calculations have been performed over planar hexahedral meshes, conveniently refined in the vicinity of the defect, which guarantees a successful accuracy and computation economy. Additional details of the method are given in Ref. [17].

As a result, this FEM model computes the bulk volumetric temperature as a function of time over the entire domain in presence of delaminations. Once the steady-state oscillatory temperature is obtained, the resulting amplitudes and phases are calculated in a further post-processing computation stage.

Overall, for the delamination geometries studied throughout this work, the numerical calculations are performed over a mesh with approximately 20,000 (average) elements in a workstation with 64 Intel® Xeon Gold 5218 2.3/3.9 GHz processors and 196 Gb RAM memory. Calculations are parallelized to 8 simultaneous computing processes and solved by using OpenFOAM [20] software. Under these conditions, the computation takes around 4 min to complete.

In order to check the consistency of both methods, analytical and numerical, we have performed an exhaustive comparison between them.

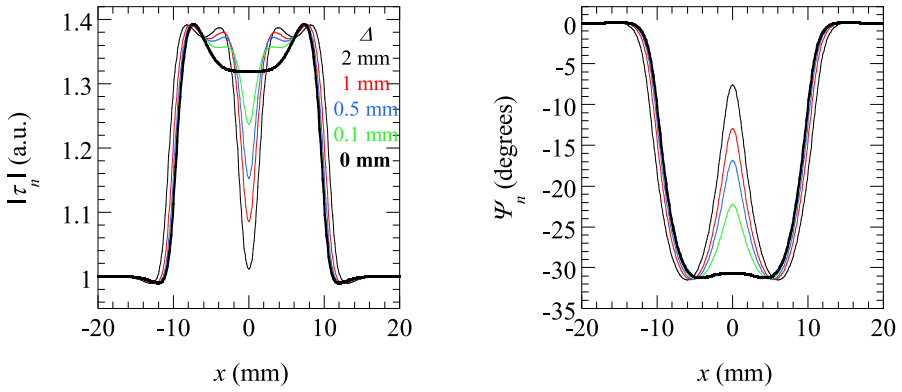

Fig. 2. Calculations of x-profiles of the amplitude and phase of the normalized surface temperature for a bulk AISI-304 sample containing two delaminations of the same length ($\ell_1 = \ell_2 = 10$ mm), depth ($d_1 = d_2 = 1$ mm) and thickness ($w_1 = w_2 = 50$ μm). Calculations are performed at $f = 0.4$ Hz. The effect of the distance between them (Δ) is analysed.

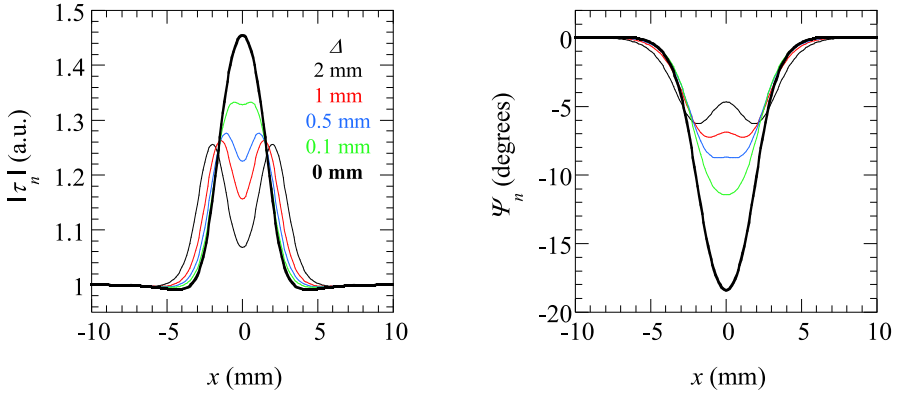

Fig. 3. The same as in Fig. 2 for shorter identical delaminations: $\ell_1 = \ell_2 = 2$ mm.

Several cases have been quantitatively analysed considering samples with two delaminations of different lengths, depths, thicknesses and distances between them. Moreover several modulation frequencies between 0.1 and 1 Hz have been studied, which is a typical range for detecting delaminations. For each pair of delaminations, we have calculated the x-profiles of the amplitude and phase of the surface temperature and we have evaluated the relative root mean square error (RMSE), which has been calculated by dividing the absolute RMSE by the norm of the temperature. In all cases, the relative RMSE is below 1 %, which shows the consistency of both analytical and numerical models.

2.3. Calculations

All calculations in this section are performed using the analytical model and for an AISI-304 stainless steel ($D = 4.0$ mm^2/s and $K = 15$ Wm^{-1}K^{-1}) thermally thick sample ($e \gg \mu$, where $\mu = \sqrt{D/(\pi f)}$ is the thermal diffusion length [21]). Although this material is not prone to delaminate, we have selected it because of its intermediate thermal properties and due to the easiness in manufacturing calibrated delaminations required to test the validity of the models, as we did in a previous work [18]. Anyway, as it will be discussed later, the conclusions of these calculations can be easily extrapolated to materials of lower or higher thermal transport properties.

First, we analyse the ability of lock-in experiments to resolve (distinguish) two close delaminations submerged at the same depth.

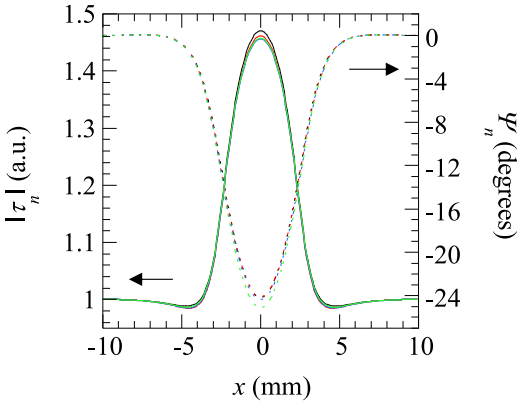

Fig. 4. Calculations of x-profiles of the amplitude (continuous lines) and phase (dashed lines) of the normalized surface temperature for a bulk AISI-304 sample containing two centred superimposed delaminations of the same length ($\ell_1 = \ell_2 = 5$ mm), thickness ($w_1 = w_2 = 50$ μm) but varying the depth. Red lines: $d_1 = 1$ mm and $d_2 = 2$ mm; blue lines: $d_1 = 1$ mm and $d_2 = 1.5$ mm and green lines: $d_1 = 1$ mm and $d_2 = 1.1$ mm. For comparison the black line corresponds to a single delamination with $d = 1$ mm. Calculations are performed at $f = 0.4$ Hz. (For interpretation of the references to colour in this figure legend, the reader is referred to the Web version of this article.)

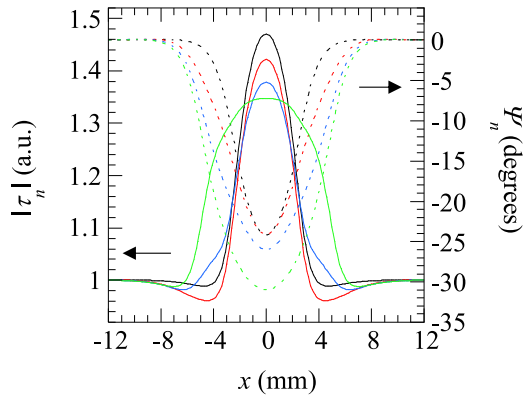

Fig. 5. The same as Fig. 4, but enlarging the length of the most submerged delamination: (ℓ_1 = 5 mm and ℓ_2 = 10 mm). For the sake of clarity, the amplitude is plotted with continuous lines and the phase with dotted lines.

Fig. 2 shows the profiles along the x-direction of the normalized surface temperature amplitude, $|\tau_n|$, and phase, Ψ_n, for a sample containing two identical delaminations of the same length ($\ell_1 = \ell_2 = 10$ mm), depth ($d_1 = d_2 = 1$ mm) and thickness ($w_1 = w_2 = 50$ μm). We have selected this thickness because we demonstrated that for a material of similar thermal diffusivity and same delaminations depth, the highest thickness sensitivity is produced in the range 10–100 μm [see Fig. 3 in Ref. [15]. Normalization is performed by dividing the complex surface temperature field by the temperature in a surface region far away from the delaminations. Calculations have been performed at f = 0.4 Hz, corresponding to a thermal diffusion length in AISI-304 μ = 1.78 mm. This is an appropriate frequency to sense delaminations buried to a depth of 1 mm. We define the distance between the delaminations as Δ, so that $\Delta = 0$ means that they are in contact. The effect of five distances Δ are shown in Fig. 2. As can be observed, both amplitude and phase are able to resolve the pair of delaminations, even though they are very close in comparison to the delamination length.

Now we analyse the case of shorter delaminations. In this frame we calculate the x-profiles of $|\tau_n|$ and Ψ_n for a bulk sample of AISI-304 containing two identical delaminations of the same geometrical properties as in Fig. 2, but for $\ell_1 = \ell_2 = 2$ mm. The same frequency is used: f = 0.4 Hz. As before, the effect of five distances Δ is analysed. The results are shown in Fig. 3. As can be observed, even for these challenging delaminations both amplitude and phase are able to resolve them, even when they are very close. It is worth noting the enhanced contrast in both amplitude and phase for $\Delta = 0$ in comparison to $\Delta = 0.1$ mm. To understand this behavior it is worth remembering that the rise of $|\tau_n|$ (and the reduction of Ψ_n) above the delamination is due to the reflection of the thermal waves generated at the sample surface and propagating through the sample (see p.19 in Ref. [21]). The presence of small holes between the delaminations reduces drastically the reflection of the thermal waves at the delamination, thus reducing the thermal contrast at the sample surface.

After analysing the case of delaminations buried at the same depth, now we study the case of superimposed delaminations. First, we deal with the case of superimposed centred delaminations of the same length. Fig. 4 shows the normalized amplitude and phase of the surface temperature for two superimposed delaminations of the same length ($\ell_1 = \ell_2 = 5$ mm), thickness ($w_1 = w_2 = 50$ μm) but varying the depth. In this figure, black lines correspond to one delamination with d = 1 mm; red lines to two delaminations with $d_1 = 1$ mm and $d_2 = 2$ mm; blue lines to two delaminations with $d_1 = 1$ mm and $d_2 = 1.5$ mm and green lines to two delaminations with $d_1 = 1$ mm and $d_2 = 1.1$ mm. Calculations are performed at $f = 0.4$ Hz. As can be observed, the surface temperature is almost insensitive to the deepest delamination, indicating that it will remain hidden in lock-in thermography experiments (see Fig. 5).

Finally, we study the case of two superimposed and centred delaminations where the deepest one is longer than the shallowest one: ℓ_1 = 5 mm and ℓ_2 = 10 mm. All the other parameters are the same as in Fig. 4. Now the shape of the x-profiles corresponding to different depths of the second delamination are very different, indicating the possibility of retrieving the parameters of both delaminations.

3. Inverse parameter estimation

Usual thermographic inversion parametric procedures are ill-posed problems due to the ambiguity resulting from the cross-correlations between the geometrical parameters of the studied defects, in this work delaminations. As a consequence, both, the lack of a sufficient sensitivity together with the potential parametric couplings often lead to a complex parameter inversion. Addressing the particular problem of the delamination geometrical determination, according to Ref. [17], even for a single delamination, its geometry cannot be successfully retrieved considering the noticeable penalization of the overall results as a function of decreasing delamination length values. This lack of sensitivity to ℓ, leaving aside other potential parametric couplings, results in a parameter estimation that easily can differ substantially from the expected values. In this frame, when multiple delaminations are considered, in principle, the inversion procedure could present a noticeably higher complexity as a function of an increasing number of unknown parameters.

3.1. Residual function analysis

Aiming at providing an insight on the aforementioned difficulties, and taking into account that the critical scenario appears when length and width are coupled [18], the behaviour of the residual function depending on these two geometrical parameters is studied. It is worth to notice that, in order to perform a fair residual ponderation between amplitude and phase, the real/imaginary parts of the thermal wave have been used to calculate the residuals, according this expression

$$r = \sum_{i=1}^{N} \left([\mathrm{Re}(\underset{\text{case}}{x_i,}) - \mathrm{Re}(x_i, \text{target})]^2 + [\mathrm{Img}(\underset{\text{case}}{x_i,}) - \mathrm{Img}(x_i, \text{target})]^2 \right) \tag{13}$$

In particular, the studied configurations consist in two identical delaminations corresponding to lengths of 2 and 10 mm, with fixed depth and width at 1 mm and 50 μm respectively and separated 0.1 mm. For the sake of clarity only two free parameters have been considered, namely ℓ and w, while the rest are considered fixed to the targeted values.

From Fig. 6, it can be seen that, in both studied cases, there is a large number of local minima even far from the global minimum in both directions ℓ and w, mainly in the last one. However, when comparing both residual maps for the two studied delamination lengths, a higher number of local minima is observed for the ℓ = 2 mm case, which indicates that shorter ℓ values lead to more complex residual distributions. In addition, in this frame, the computed residuals corresponding to each local minima can be hardly distinguishable between them and also with the global minimum.

It must be noted that this conclusion corresponds to the mentioned ℓ and w free parameter identical delamination case. However, even a more adverse residual distribution can be obtained if a larger set of free parameter inversion is sought, systematic errors are included or experimental noise is incorporated to the calculation. In these cases, the aforementioned phenomenology is worsen. As a consequence, an inverse parametric estimation based on a local minimization procedure, such as Steepest Descent method, would be highly dependent on the initial guess, and therefore could potentially lead to an inaccurate estimation of the real geometry of the delaminations. Accordingly, an

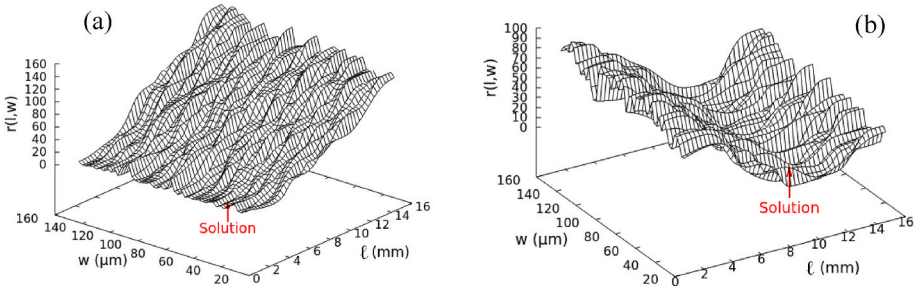

Fig. 6. Dependence of the residual function on ℓ and w for two pair of identical delaminations: (a) $\ell_1 = \ell_2 = 2$ mm, $d_1 = d_2 = 1$ mm, $w_1 = w_2 = 50$ μm and $\Delta = 0.1$ mm and (b) $\ell_1 = \ell_2 = 10$ mm, $d_1 = d_2 = 1$ mm, $w_1 = w_2 = 50$ μm and $\Delta = 0.1$ mm. Calculations are performed for $f = 0.4$ Hz.

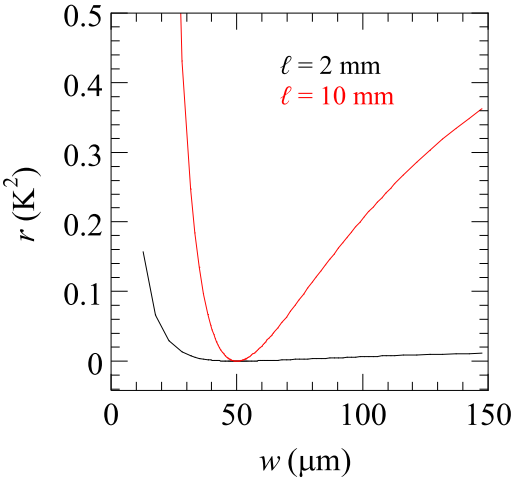

Fig. 7. Dependence of the residual function on w for two pair of identical delaminations with fixed $d = 1$ mm and $\Delta = 0.1$ mm. Calculations are performed for $f = 0.4$ Hz.

appropriate inversion procedure must be developed in order to guarantee that the global minimum is reached.

In addition to the unavoidable presence of local minima in the residuals distribution as a function of the length and width of the delaminations, the sensitivity to the target parameters must also be considered. One estimation of this sensitivity can be carried out by measuring the concavity of the global minimum in the residual distribution. Since the addressed problem presents a high complexity in these terms, for clarity, the sensitivity to a single parameter can be analysed in order to determine the ability of the inversion procedure to correctly determine the targeted values. Since the width of the delamination is the parameter suffering a larger penalization depending on the estimation of the other parameters [17], r (w) will be studied. With this objective, in Fig. 7, it can be seen the comparison between two configurations of identical delaminations with $\ell = 2$ and 10 mm, $d = 1$ mm, $\Delta = 0.1$ mm.

From the results shown in Fig. 7 it can be concluded that for decreasing lengths the residual curves are flattened, meaning that for the shortest delamination studied, large w value differences can lead to very small residual differences. Therefore, as a general rule, the retrieval of the global minimum for small delamination length values can only be attained by means of a very strict minimization threshold value. Even in this case, only ideal retrievals might be successfully accomplished, since the presence of noise, systematic errors or other error sources could easily disguise the target global minimum.

3.2. Inverse parametric estimation procedure and results

The aim of this section is to develop a method for sizing the morphological features of multiple delaminations: lengths, depths, thicknesses and the separation between them. In these regards, the difficulties introduced by the presence and the nature of the local minima addressed in subsection 3.1 must be necessarily overcome. Based on the versatility of the developed FEM formulation, we propose an inverse parametric estimation consisting in a residual multi-parametric minimization problem between the numerical model and experimental results as a function of the unknown parameters. In this frame, a double step constrained residual minimization procedure to reach the global true solution, regardless the evaluation initial guess is proposed. First, a stochastic global optimization stage is performed based on the DIRECT algorithm [22]. This procedure allows reaching a solution close to the global minimum up to a pre-selected arbitrary tolerance. The search is constrained based on a minimum residual value without discarding any other regions of the probe space during the searching process. Once the stopping criterion is satisfied, starting from the global algorithm solution, a faster local minimization is performed by means of a generalized Levenberg-Marquardt [24,25], namely NL2SOL algorithm [23]. It must be noticed that following the residual calculation criteria detailed in subsection 3.1, the real and imaginary part of the thermal wave have been used.

The presented optimization algorithm has been deployed in the search of morphological parameters corresponding to two delaminations. After solving the corresponding direct heat transfer problem, statistical Gaussian noise has been added to reproduce realistic surface temperature values. According to the analysis presented in Ref. [26], 1 mK Gaussian noise has been added, which is equivalent to recording at least 2000 images (e.g. 100 images/s for 20 s) for the lock-in process.

Fig. 8 shows noisy synthetic temperature x-profiles in a thermally thick AISI-304 containing two subsurface delaminations. The sample is illuminated by a homogeneous light source of intensity $I_o = 6250$ W/m^2 modulated at $f = 0.4$ Hz, which induces a surface temperature oscillation amplitude of 0.26 K in a region far away from the delamination, a very realistic value in lock-in experiments. In all plots the dots are the synthetic data and the continuous lines correspond to the results from the direct model which minimizes the residual function after the inversion process. For the sake of clarity, temperature amplitude and phases are shown instead of the real and imaginary parts used for the inversion. Four cases depending on the length, depth, width and separation between the delaminations are studied.

Fig. 8a corresponds to two subsurface delaminations buried at the same depth with the following parameters: $\ell_1 = 10$ mm, $\ell_2 = 5$ mm, $d_1 = d_2 = 1.5$ mm, $w_1 = 50$ μm, $w_2 = 25$ μm and $\Delta = 0.1$ mm. Fig. 8b refers to a similar but most challenging case since the delaminations are shorter: $\ell_1 = \ell_2 = 2$ mm, $d_1 = d_2 = 1$ mm, $w_1 = 50$ μm and $\Delta = 0.1$ mm. In both cases the delaminations are very close with the aim of verifying the capability of lock-in thermography two resolve them. Fig. 8c stands

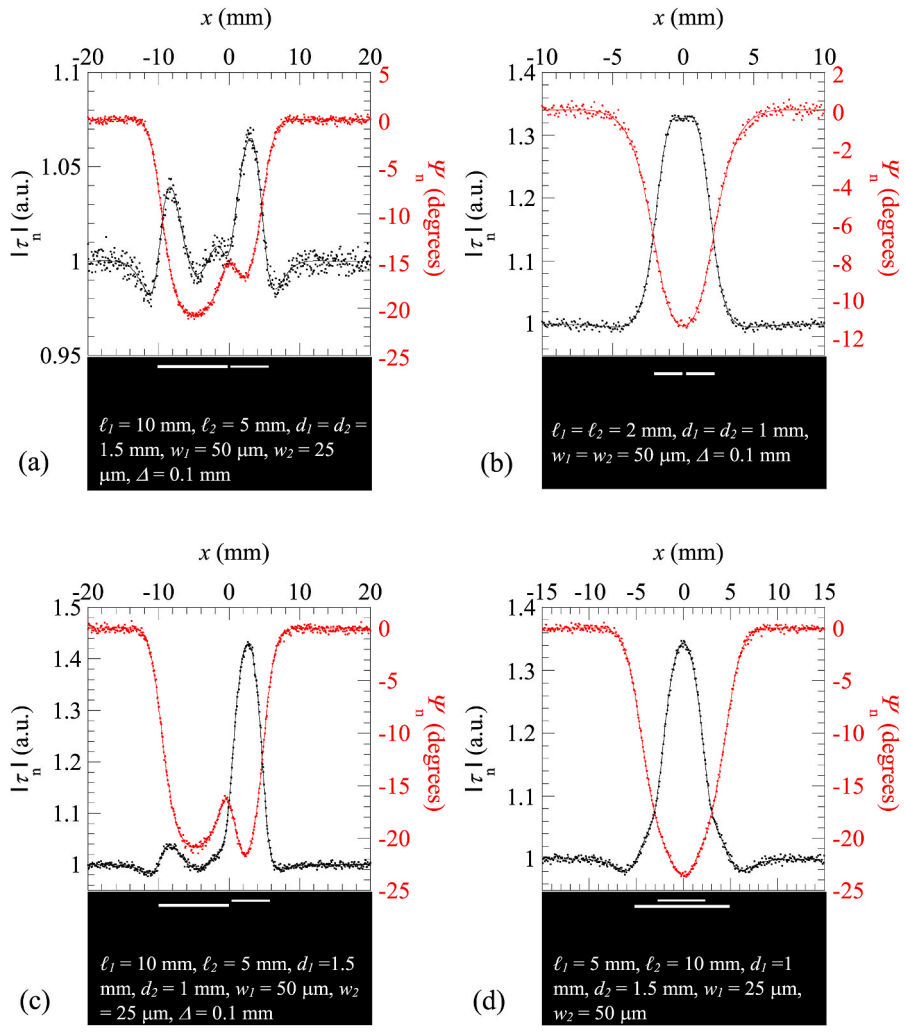

Fig. 8. Noisy synthetic temperature x-profiles (dots) and inverse multi-parametric estimations (continuous lines). Common parameters: bulk AISI-304, $I_o = 6250$ W/m^2 and $f = 0.4$ Hz. Below each plot a scheme of the position of the delaminations is included.

Table 1
Retrieved delaminations lengths (ℓ), depths (d) and thicknesses (w) for the 4 cases studied in this work.

		ℓ_1 (mm)	d_1 (mm)	w_1 (μm)	ℓ_2 (mm)	d_2 (mm)	w_2 (μm)	Δ (mm)
2 long same depth delaminations	Real	10.00	1.50	50	5.00	1.50	25	0.10
	Retrieved	10.00 ± 0.01	1.50 ± 0.01	49 ± 2	5.01 ± 0.02	1.50 ± 0.01	25 ± 1	0.10 ± 0.01
2 short same depth delaminations	Real	2.00	1.00	50	2.00	1.00	50	0.10
	Retrieved	2.06 ± 0.02	0.997 ± 0.002	20 ± 5	2.02 ± 0.02	1.005 ± 0.002	32 ± 6	0.07 ± 0.01
2 different depth delaminations	Real	10.00	1.50	50	5.00	1.00	25	0.10
	Retrieved	10.01 ± 0.01	1.50 ± 0.01	50 ± 2	5.01 ± 0.01	1.00 ± 0.01	25 ± 1	0.09 ± 0.01
2 superimposed centred delaminations	Real	5.00	1.00	25	10.00	1.50	50	–
	Retrieved	5.00 ± 0.01	1.00 ± 0.01	25 ± 1	9.98 ± 0.02	1.50 ± 0.01	51 ± 6	–

Note that we have kept the modulation frequency fixed for the four cases. This means that even better results would have been obtained if a frequency scan had been performed with the aim of finding the most sensitive frequency for each configuration.

for two delaminations buried at different depth, but the upper one does not overshadow the deepest one: $\ell_1 = 10$ mm, $\ell_2 = 5$ mm, $d_1 = 1.5$ mm, $d_2 = 1$ mm, $w_1 = 50$ μm, $w_2 = 25$ μm and $\Delta = 0.1$ mm. Finally, Fig. 8d deals with two superimposed and centred delaminations: $\ell_1 = 5$ mm, $\ell_2 = 10$ mm, $d_1 = 1$ mm, $d_2 = 1.5$ mm and $w_1 = 25$ μm, $w_2 = 50$ μm. The obtained geometrical parameters using the multi-parametric procedure described before are summarized in Table 1. As can be observed, the agreement is excellent for cases (a), (c) and (d), for which all the parameters are obtained with high accuracy and very small uncertainty. In case (b), corresponding to short delaminations, not all the parameters are obtained with the same accuracy. Depths are exact (error <1 %). Lengths are obtained with good accuracy showing just a slight overestimation (error <2 %). Accordingly, the distance between delaminations, Δ, is slightly underestimated because the centres of the delaminations remain unchanged. Finally, the thicknesses are clearly underestimated (error ≈ 20–35 %). This is due to the low sensitivity of the surface temperature to this parameter and, moreover, the penalization suffered by the delamination width even for slightly inaccurate length calculation, as it was already shown in the case of a single short delamination [17].

In Fig. 9 we show by dots the same noisy synthetic temperature x-profiles as in Fig. 8b, corresponding to two short delaminations of the

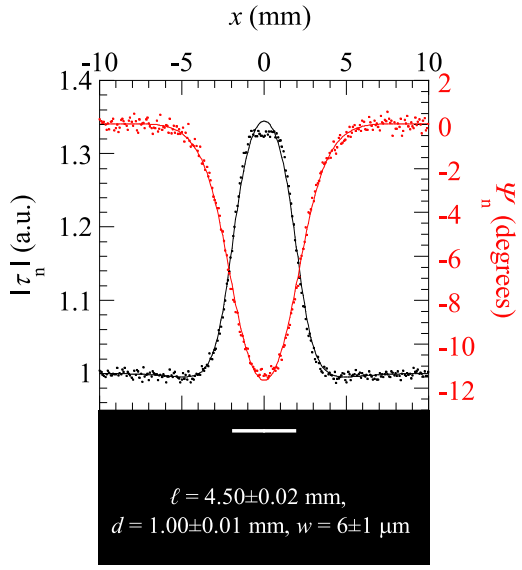

Fig. 9. The same noisy synthetic temperature *x*-profiles (dots) as in Fig. 7b, but fitted to a single delamination. The retrieved parameters are given in the inset.

same length, depth and width. The continuous lines are the best inverse parameter estimation to a single delamination. As can be observed, they follow quite well the data except for the normalized amplitude at the centre of the delamination. The retrieved results are: $\ell = 4.50 \pm 0.02$ mm, $d = 1.00 \pm 0.01$ mm and $w = 6 \pm 1$ μm. Note that the obtained length is longer than $\ell_1 + \ell_2 + \Delta = 4.1$ mm while the width remains clearly underestimated. Finally, and what is more significant, the residuals corresponding to the fitting to two delaminations, 0.00105 K^2, are smaller than the residuals for a single delamination, 0.00167 K^2. Accordingly, we can conclude that the inversion algorithm unambiguously indicates that there are two delaminations and not a single one.

In this work, all calculations have been performed for AISI-304 stainless steel, a material with intermediate thermal transport properties. The behaviour for good and bad thermal conductors depends on both *D* and *K*. On the one hand, thermal diffusivity governs the thermal diffusion length, $\mu = \sqrt{D/(\pi f)}$, i.e. the penetration of the thermal wave, which governs both depth sensitivity and resolution capability. From the expression it can be seen that *D* and *f* are correlated. This means that for Zn, which has a thermal diffusivity 10 times higher than AISI-304, the same thermal wave penetration is reached by a frequency 10 times higher. Contrarily, for glass, which has a thermal diffusivity 10 times lower than AISI-304, the same thermal wave penetration is reached by a frequency 10 times lower. On the other hand, the amplitude and phase contrast for a given thickness of the delamination depends on *K*, or better said, on the ratio between *K* and K_{air}, which controls the thermal resistance of the delamination. In this way, the higher the thermal conductivity of the sample, the higher the thermal contrast of the delamination. This means that thin delaminations are better detected in good thermal conductors.

As a final remark let us remember that in these simulations only statistical noise has been added. In real experiments systematic errors, such as non-uniform illumination, surface heterogeneities, stray light, etc., may limit the accuracy of the results. Accordingly, the accuracy obtained in this work should be considered as an upper limit in the precision of the retrieved geometrical parameters of the delaminations.

4. Conclusions

In this article we addressed the nondestructive characterization of a material that contains several parallel delaminations using lock-in IRT. First, we have calculated, both analytically and numerically, the surface temperature oscillation of an opaque material containing several subsurface parallel delaminations. We have verified that both methods deliver the same temperature profiles with a precision better than 1 %. Then we have performed surface temperature calculations for an opaque sample containing two delaminations. Two configurations have been analysed. In the first one, both delaminations are buried at the same depth. We found that they can be resolved even though they are very close. In the second configuration both delaminations are superimposed. In this case they can be resolved provided the shallowest one does not overshadow the deepest one completely.

The second part of this work is devoted to sizing the geometrical parameters of both delaminations (lengths, depths, thicknesses and the separation between them). The analysis of the residual function corresponding to synthetic temperature data indicated that there are plenty of local minima far away from the true solution and that the sensitivity to the delamination thickness is smaller than the sensitivity to the other parameters, mainly for short delaminations. These results suggested that an inverse parametric estimation based on a local minimization procedure, such as Steepest Descent method, could lead to inaccurate reconstruction of the morphology of the delaminations. Accordingly, we have developed a double step constrained residual minimization procedure: a stochastic global optimization stage to reach a solution close to the global minimum, followed by a local minimization using a generalized Levenberg-Marquardt algorithm. We have tested the validity of this inverse procedure on synthetic temperature data with added statistical noise. In all cases, we retrieved depths, lengths and separation of the delaminations with high accuracy. As expected from the sensitivity analysis, the thicknesses are obtained with less precision, which diminishes as the lengths are shortened. Anyway, it is remarkable the ability of this methodology to characterize delaminations with thicknesses of just a few tens of microns. Finally, we verified that two very close delaminations are clearly distinguished from a single one.

Funding

This work has been supported by Departamento de Educación del Gobierno Vasco (IT1430-22). This work was carried out within the framework of the Joint Cross-Border Laboratory (LTC) AENIGME (Aquitaine Euskadi Network in Green Manufacturing and Ecodesign). The authors would like to thank the Basque Government and EUSKAMPUS (LTC Sarea innitiative) for their financial support for this LTC and this research work.

CRediT authorship contribution statement

A. Salazar: Writing – original draft, Methodology, Conceptualization. **D. Sagarduy-Marcos:** Writing – review & editing, Software, Investigation. **J. Rodríguez-Aseguinolaza:** Writing – original draft, Software, Investigation. **A. Mendioroz:** Writing – review & editing, Methodology. **J.C. Ciria:** Software, Investigation. **R. Celorrio:** Software, Conceptualization.

Declaration of competing interest

Authors declare that there is not any conflict of interest.

Data availability

Data will be made available on request.

References

[1] Maldague XPV. Theory and practice of infrared technology for nondestructive testing. New York: John Wiley & Sons; 2001.
[2] Askaripour K, Zak A. A Survey of scrutinizing delaminated composites via various categories of sensing apparatus. J. Compos. Sci. 2019;3:95.

[3] Shepard SM, Lhota JR, Rubadeux BA, Ahmed T, Wang D. Enhancement and reconstruction of thermographic NDT data. Proc SPIE 2002;4710:531.
[4] Rajic N. Principal component thermography for flaw contrast enhancement and flaw depth characterization in composite structures. Compos Struct 2002;58:521.
[5] Balageas DL. Defense and illustration of time-resolved pulsed thermography for NDE. QIRT Journal 2012;9:3.
[6] Sun J. Analysis of data processing methods for pulsed thermal imaging characterisation of delaminations. QIRT J. 2013;10:9–25.
[7] Angioni SL, Ciampa S, Pinto E, Scarselli G, Almond DP, Meo M. An analytical model for defect depth estimation using pulsed thermography. Exp Mech 2016;56:1111–22.
[8] D'Accardi E, Palano F, Tamborrino R, Palumbo D, Tati A, Terzi R, Galietti U. Pulsed phase thermography approach for the characterization of delaminations in CFRP and comparison to phased Array Ultrasonic testing. J. Nondestruct. Eval 2019;38:1.
[9] Wu D, Busse G. Remote inspection of wood with lock-in-thermography. Tappi J 1996;79:119–23.
[10] Ekanayake S, Gurram S, Schmitt RH. Depth determination of defects in CFRP-structures using lock-in thermography. Compos B Eng 2018;147:128–34.
[11] Toscano C, Riccio A, Camerlingo F, Meola C. On the use of lock-in thermography to monitor delamination growth in composite panels under compression. Sci. Eng. Compos. Mat. 2014;21:485–92.
[12] Feuillet V, Ibos L, Fois M, Dumoulin J, Candau Y. Defect detection and characterization in composite materials using square pulse thermography coupled with singular value decomposition analysis and thermal quadrupole modelling. NDT&E Int. 2012;51:58–67.
[13] Müller JP, Dell'Avvocato G, Krankenhagen R. Assessing overloaded-induced delaminations in glass fiber reinforced polymers by its geometry and thermal resistance. NDT&E Int. 2020;116:102309.
[14] Groz MM, Bensalem M, Sommier A, Abisset-Chavanne E, Chevalier S, Chulkov A, Battaglia JL, Batsale JC, Pradere C. Estimation of thermal resistance field in layered materials by analytical asymptotic method. Appl Sci 2020;10:2351.
[15] Salazar A, Mendioroz A. Sizing the depth and thickness of ideal delaminations using modulated photothermal radiometry. J Appl Phys 2022;131:085106.
[16] Maillet D, André S, Batsale JC, Degiovanni A, Moyne C. Thermal quadrupoles. New York: Wiley; 2000 [chapter 6].2.
[17] Salazar A, Sagarduy-Marcos D, Rodríguez-Aseguinolaza J, Mendioroz A, Celorrio R. Characterization of semi-infinite delaminations using lock-in thermography: theory and numerical experiments. NDT&E Int. 2023;138:102883.
[18] Sagarduy-Marcos D, Pérez-Arbulu J, Rodríguez-Aseguinolaza J, Mendioroz A, Batsale JC, Salazar A. Characterization of semi-infinite delaminations using lock-in thermography: experimental results. NDT&E Int 2023;138:102903.
[19] Carslaw HS, Jaeger JC. Conduction of heat in Solids. second ed. Oxford: Oxford University Press; 1959. p. 20.
[20] Weller HG, Tabor G, Jasak H, Fureby C. A tensorial approach to computational continuum mechanics using object-oriented techniques. Comput Phys 1998;12:620.
[21] Almond DP, Patel PM. Photothermal Science and techniques. London: Chapman & Hall; 1996. p. 15.
[22] Perttunen CD, Jones DR, Stuckman BE. Lipschitzian optimization without the Lipschitz constant. J. Optim. Theory Appl. 1993;79:157.
[23] Dennis Jr JE, Gay DM, Welsch RE. An adaptive nonlinear least-squares algorithm. ACM Trans. Math. Softw. 1981;7:348.
[24] Levenberg K. A method for the solution of certain non-linear problems in least squares. Quarterly of Appl. Math. 1944;2:164–8.
[25] Marquardt DW. An algorithm for least-squares estimation of nonlinear parameters. J. Soc. Indust. Appl. Math. 1963;11:431–41.
[26] Breitenstein O, Langenkamp M. Lock-in thermography. Berlin: Springer; 2003. p. 32.